Available online at www.sciencedirect.com

SciVerse ScienceDirect

Journal of the European Ceramic Society 32 (2012) 3929–3939

www.elsevier.com/locate/jeurceramsoc

Mechanical behavior characterization of high zirconia fused-cast refractories at high temperature: Influence of the cooling stage on microstructural changes

C. Patapy [a,**], N. Gey [c], A. Hazotte [c], M. Humbert [c], D. Chateigner [d], R. Guinebretiere [e], M. Huger [a,**], T. Chotard [a,b,*]

[a] *Groupe d'Etude des Matériaux Hétérogènes (GEMH), Centre européen de la Céramique (CEC), 12 rue Atlantis, 87068 Limoges Cedex, France*
[b] *IUT du Limousin, Département GMP, 2 Allée A. Maurois, 87065 Limoges Cedex, France*
[c] *Laboratoire d'étude des microstructures et de mécanique des matériaux (LEM3) UMR CNRS 7239, Ile du Saulcy, 57045 Metz – cedex 01, France*
[d] *Laboratoire de cristallographie et sciences de matériaux (CRISMAT), UMR CNRS 6508,6 Boulevard du Maréchal Juin – F-14050 Caen cedex 4, France*
[e] *Laboratoire de Science des procédés céramiques et traitement de surface, (SPCTS) UMR CNRS 6638, Centre européen de la Céramique (CEC), 12 rue Atlantis, 87068 Limoges Cedex, France*

Available online 2 June 2012

Abstract

Today, the high quality level required by new applications of glass, imposes the use of high zirconia refractories (HZ). These are designed to operate in extreme condition and also require control of the making process. Elaborated by a fused cast process followed by a controlled cooling step, these materials exhibit specific thermo mechanical properties related to a microstructure containing monoclinic zirconia dendrites embedded into a silica–alumina glassy phase.

The present paper deals with the understanding of damage phenomena at a low scale during the cooling process after cast-fusion. Mechanical characterizations at high temperature are carried out to identify the chronology of the microdamage. Microstructure observations using SEM and EBSD complete thermal experiments and allow to identify main characteristics of microdamage mechanisms. This work was conducted in the framework of a French national research program "NOREV", aiming to build numerical tools to optimize the casting process of such materials.

Keywords: E. Refractories; C. Mechanical properties; C. Thermal expansion; D. ZrO_2

1. Introduction

Fused-cast refractory materials are widely used in glass furnaces to prevent from corrosion effects of the melting glass. Such a quality is especially due to the low opened porosity of these materials. First generations of these products were alumina–zirconia–silica compounds (in proportions located in the eutectic domain), which appear to be well adapted for soda-lime products.[1] Since three decades, other compositions have been developed to answer to special needs for the casted glass and the process. Thereby, products with a high content of zirconia (>92 wt%) have been improved for the manufacturing of special technical glasses (for LCD screens, lead crystal, ...) and very corrosive glasses (boron-silicate glasses, ...).[2] If the improvement added by such a technology is clearly identified today in glass manufacturing campaigns, it remains some difficulties to obtain easily large refractory blocks after the fused-casting process. In fact, the elaboration consists in cooling from 2400 °C to room temperature a material which solidifies in a two-phased structure (zirconia and a glassy phase), each of these phases having different thermal expansions and thus creating thermal mismatches. Moreover, during the cooling process, zirconia transforms successively through cubic, tetragonal and monoclinic form, with tetragonal and monoclinic forms exhibiting anisotropy in thermal expansion along their crystallographic axes. The resulting complex microstructure is made of numerous different crystallographic domains called variants. Finally,

* Corresponding author at: Groupe d'Etude des Matériaux Hétérogènes (GEMH), Centre européen de la Céramique (CEC), 12 rue Atlantis, 87068 Limoges Cedex, France. Tel.: +33 5 87 50 25 60.
** Corresponding authors.
E-mail addresses: cedric.Patapy@Epfl.Ch (C. Patapy), marc.huger@unilim.fr (M. Huger), thierry.chotard@unilim.fr (T. Chotard).

0955-2219/$ – see front matter © 2012 Elsevier Ltd. All rights reserved.
http://dx.doi.org/10.1016/j.jeurceramsoc.2012.04.043

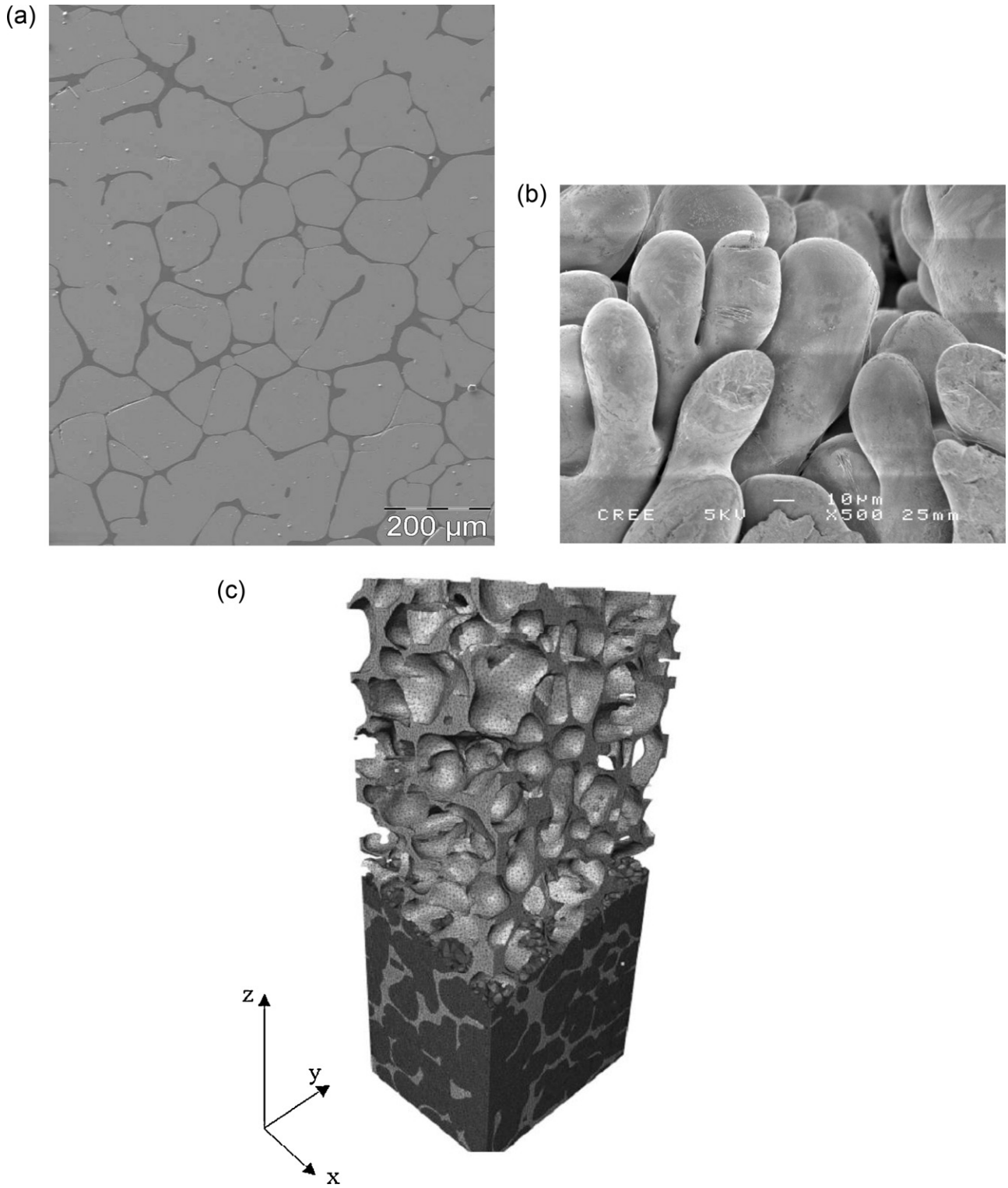

Fig. 1. SEM observations of the microstructure with zirconia grains in gray and the glassy phase in black (a), of the dendritic structure of zirconia revealed after HF attack (b) and 3D microstructure of a fused-cast refractory material with a high content of zirconia observed by X-Ray tomography (c).[3]

and maybe the most critical effect, the shift from the tetragonal to the monoclinic structure is responsible for a large volume expansion (typically 4%).

This effect explains the inability to produce sintered materials containing undoped zirconia. The material obtained after the fusion cast process presents some microcracks due to the stress relaxation during the cooling process. The manufacturing process must be rigorously controlled, in particular the cooling rate after fusion, in order to limit mechanical stresses (source of possible damage) induced by important thermal gradients and the martensitic tetragonal–monoclinic transformation of zirconia.[3]

This paper aims to identify the nature and the way of microcracking occurrence during the cooling process. Elastic properties, closely related to the occurrence of microdamage, are studied with two different methods operating at high temperature: an ultrasonic and a tensile test device. These thermo-mechanical data are completed with thermal expansion and acoustic emission analysis. They allow to investigate accurately the influence of the cooling process on microstructure changes. All of these treatments are performed down from 1500 °C (after a first heating), and will be discussed in correlation with microstructure observations at room temperature using SEM and Electron BackScattering Diffraction.

2. Materials

The studied material is a fused-cast refractory containing 94 wt% of ZrO_2 monoclinic crystals and 6 wt% of a borosilicate glassy phase (80 wt% SiO_2, 13 wt% Al_2O_3, 7 wt% B_2O_3). It exhibits a 3D microstructure with dendrites of zirconia embedded into a glassy phase. This microstructure is typical of metallic alloys obtained by a foundry process (lingots) (Fig. 1).

This particular organization for a ceramic material, explains both the high resistance against corrosion and the ability to resist mechanically to the transformation of zirconia tetragonal–monoclinic at around 1000 °C. In fact, the glassy phase accommodates the large volume expansion (4%) of zirconia crystals during the transition.

Materials are typically obtained under the form of large blocks (1 m^3). They are obtained by a melting process in arc furnaces followed by a controlled cooling step in molds. Finally, the block is gradually put in temperature of service for glass manufacturing. In the present paper, authors will only focus on the study of cooling stages of the casting process. Microstructure features, which are associated to the cooling, are very complex. Fig. 2a and b illustrates the different steps of microstructure evolution and the corresponding phase diagram ZrO_2–SiO_2.[4] Dendrites of zirconia initially grow under the form of the cubic structure (C) with primary and secondary ramifications (tree structure) and probably transforms into tetragonal domains (T) at around 2300 °C. Down to 1700 °C, the mixing is not supposed to be fully solid, and nucleation-growth of zirconia dendrites probably goes on in this temperature range. Below 1700 °C, the material can be considered as fully solid with zirconia dendrites embedded in silicate a glassy phase, with some traces of crystalline zircon. Between 1000 °C and 900 °C, the martensitic transformation of zirconia from the tetragonal structure to the monoclinic one (M) occurs (Fig. 3).

The cubic to tetragonal transformation is associated to a 45° rotation of the $\vec{a}$ and $\vec{b}$ axis around the $\vec{c}$ axis ($Fm\bar{3}m \rightarrow P4_2/nmc$ space group change). It induces the possible formation of three distinct crystallographic variants from one single cubic crystal. Using the pseudo-cubic lattice, axis $\overrightarrow{C_C}$ can become $\overrightarrow{a_t}$, $\overrightarrow{b_t}$ or $\overrightarrow{c_t}$.

During the tetragonal to monoclinic transformation, it is possible to form 24 different crystallographic variants. In fact there are two possible orientation relationships and eight

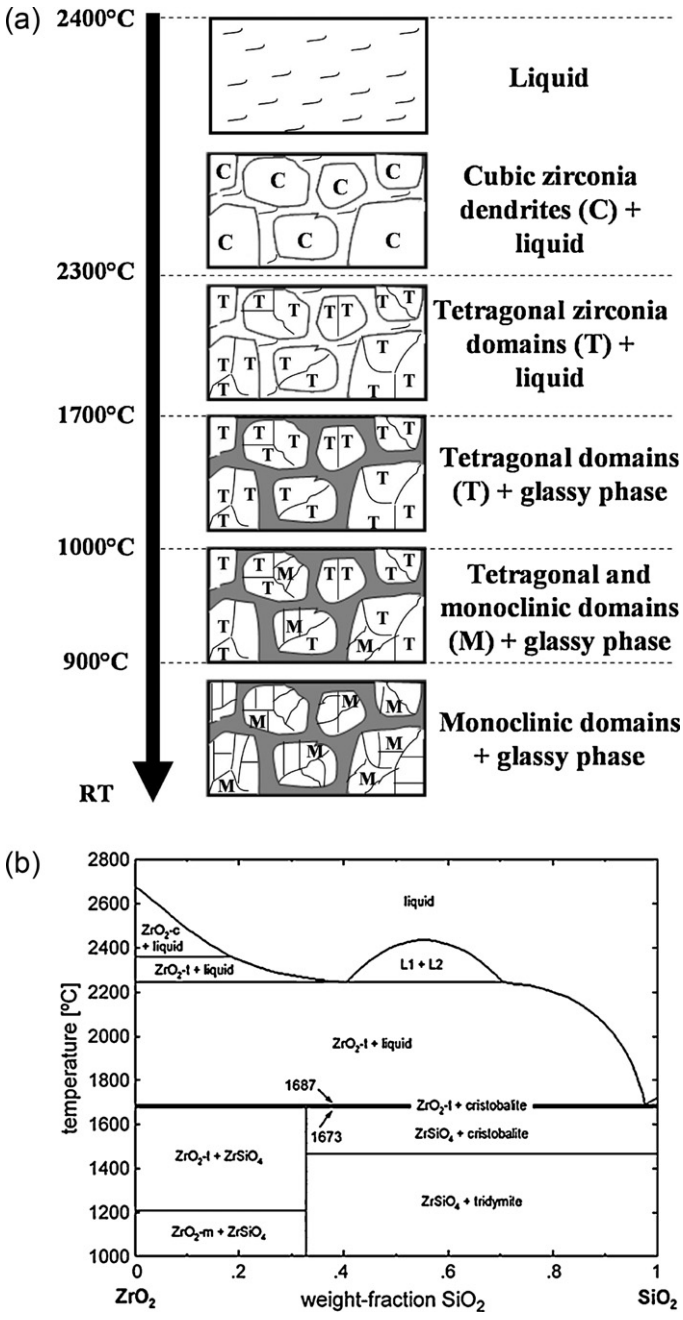

Fig. 2. Microstructure evolution during the cooling process.

crystallographic variants for each case: $\overrightarrow{c_t} - \overrightarrow{a_m}$ noted A, $\overrightarrow{c_t} - \overrightarrow{b_m}$ noted B and $\overrightarrow{c_t} - \overrightarrow{a_m}$ noted C. The monoclinic zirconia space group is $P2_1/c$ and then the β angle differs from 90° (it is close to 99°). Thus considering one specific tetragonal and monoclinic respective orientation, only two crystallographic axes of the monoclinic lattice can be parallel to a tetragonal axis: the $\overrightarrow{b_m}$ axis and the $\overrightarrow{a_m}$ or $\overrightarrow{c_m}$ one. However, the total number of possibilities is divided by two since variants can be regrouped as equivalent crystallographic pairs by rotation of 180° around $\overrightarrow{b_m}$.[5,6]

At room temperature each zirconia dendrite is therefore constituted of different monoclinic variants. Considering

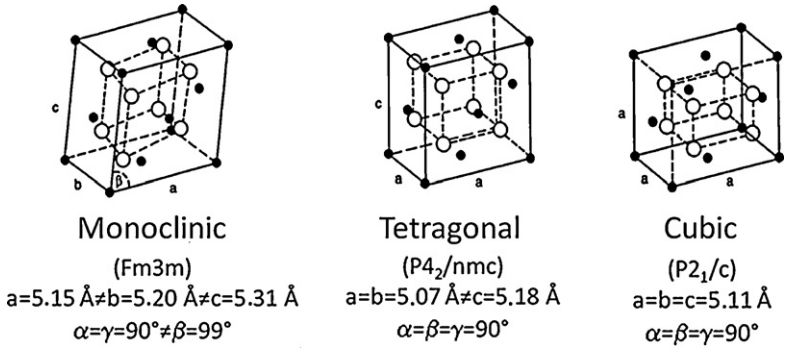

Fig. 3. Microstructure evolution during the cooling process.

the anisotropy in thermal expansion (TE) along the different crystallographic axes in the monoclinic structure, these different crystallographic variants induce thermal mismatches and then potential microcracking phenomena between variants.[7] The glassy phase within the microstructure is assumed, because of its low viscosity at this temperature, to accommodate internal stresses induced by the anisotropic expansion mismatch between ZrO_2 grains during this transformation. Nevertheless, the transformation of zirconia, combined with TE mismatches between the glassy phase and zirconia, induces microcracking.

3. Experimental techniques

3.1. High temperature ultrasonic pulse echography

An ultrasonic technique based on the continuous in situ measurement of the velocity of ultrasonic longitudinal long bar mode has been used to monitor the evolution of Young's modulus. The principle is described elsewhere.[8] To achieve satisfactory propagation conditions in this particular ultrasonic mode and taking into account the characteristics of the material, the central frequency of the pulse is 110 kHz and specimens are parallelepipeds of 5.5 mm × 5.5 mm × 100 mm. The measurement of the round trip time between two successive echoes within the sample allows to calculate the wave velocity and then to obtain the value of the Young's modulus by $E = \rho(2L/\tau)^2$ where L and ρ are sample length and density respectively.

Ultrasonic measurements of Young's modulus have been performed during thermal cycles made at a rate of 5 °C/min for heating and cooling stages and a 1 h isothermal dwell at 1500 °C.

3.2. Tensile tests

Tensile tests have been performed at room temperature with an INSTRON 8862 electro-mechanical universal testing machine which can also work at high temperature up to 1600°.[9] Strain is evaluated from the variation of a 25 mm gauge length measured by two extensometers equipped by silicon carbide rods which are placed on two opposite faces of the specimen.

The low values of the displacement at rupture exhibited by these materials (3–5 μm) required a good control of the thermal stability of extensometers. Refractory samples are constituted of a cylindrical rod (16 mm in diameter) glued to two metallic parts. The precise final geometry is obtained thanks to a cylindrical machining step of the global assembly.

3.3. High temperature acoustic emission technique

Acoustic emission (AE) is defined as "the class of phenomena whereby transient elastic waves are generated by the rapid release of energy from localized sources within the material (or structure) or the transient waves so generated".[10] When a material is subjected to mechanical or thermal stresses, acoustic emission can be generated by a variety of sources such as including crack nucleation and propagation, multiple dislocation slip, twinning, grain boundary sliding, Barkhausen effect (realignment or growth of magnetic domains), phase transformations in alloys, debonding of fibers in composite materials or fracture of inclusions in alloys or twinning for example.[11–15] It has been used either at the laboratory level or at the industrial scale. Usually, this technique is applied as a non-destructive characterization technique in order to follow in real-time the evolution of the damage of a material subjected to mechanical loading.[16–18] Others new applications of this technique have been recently developed.[19–22] The originality of this technique developed in the GEMH laboratory lies in the in situ microstructural evolution indirect-monitoring at high temperature. Here, the device aims to characterize the damage evolution and the chronology of microstructural changes occurring during thermal cycles.

A wide-band sensor (175 kHz–1 MHz) (PAC MICROPHONE μ80), connected to a preamplifier (EPA 1220A), collects, through an alumina wave-guide, the whole of the signal induced by the elastic waves released within the sample (5.5 mm × 5.5 mm × 25 mm). To avoid parasitic noises from coupling material, a direct contact between the sample and the wave-guide is set. A threshold of 35 dB has been chosen in order to filter background noise. The signal is then amplified and treated by a Mistras acquisition device from Euro Physical Acoustics Company. This system allows the waveform (hit) and the main feature parameters well known in AE study as count, hit, rise time, duration of hit, count to peak, amplitude (in dB) or signal energy, to be recorded. AE parameters have been recorded during the same heating–cooling cycles than those which were used for ultrasonic measurements.

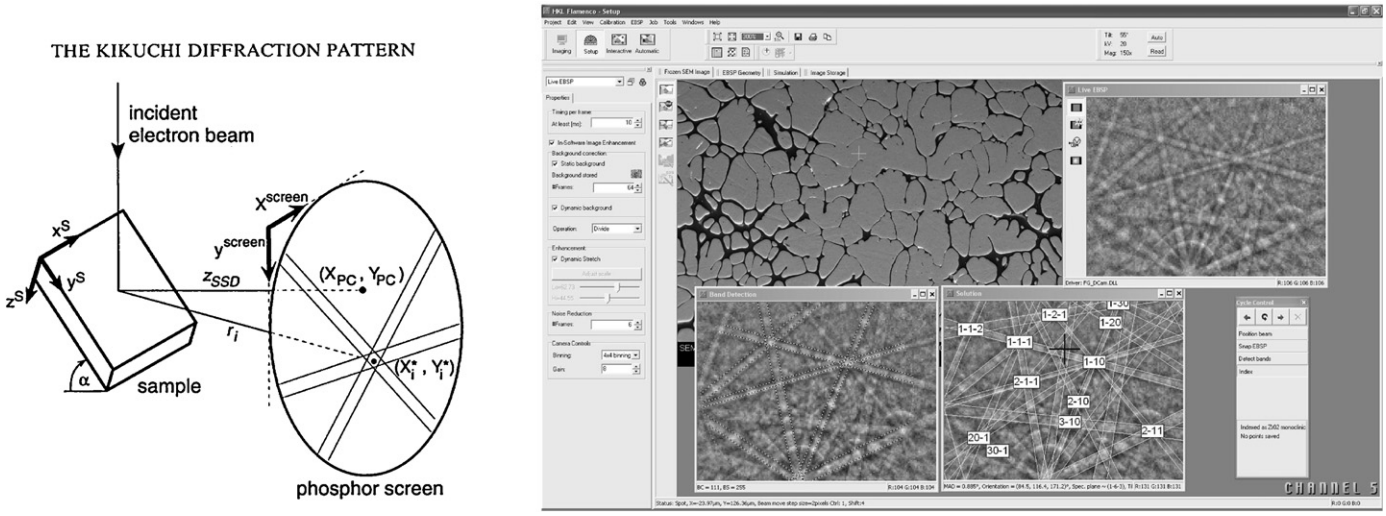

Fig. 4. Formation of Kikuchi patterns by EBSD investigations.

3.4. Electron backscattering diffraction (EBSD)

The EBSD technique is based on automatic analysis of Kikuchi-type diffraction patterns generated by backscattered electrons.[23,24] For each point of analysis, the crystallographic orientation is determined after indexing of the corresponding diffraction (Kikuchi) patterns (Fig. 4). The local textures of the sample, i.e. the different orientations of crystals compared to the sample reference, were determined using the electron back-scattering diffraction (ESBD) technique in a 6500F JEOL FEG-SEM equipped with the Channel 5 system (HKL Technology, Denmark).

Local orientations in the reference sample are often represented under the form of direct pole figure, each pole figure corresponding here to orientations of a family plane. For each analyzed crystal, this one is put on the center of a sphere pole referenced with sample axis. The present example of Fig. 4 concerns a cubic structure, which explains why three poles exist for a given family plane. In fact, in such geometry the family planes {0 0 1} regroups the three equivalent planes (1 0 0), (0 1 0) and (0 0 1). For a given crystal exhibiting a monoclinic structure for example, the same family plane will create only one pole on the pole figure due to the non equivalence of the three previous planes.

4. Results and discussion

Following results concern investigations performed with different techniques working at high temperature in order to look at microdamage mechanisms as a consequence of the evolution of thermo-mechanical properties. Elastic properties obtained by an ultrasonic method and a tensile test device are first compared. Then thermal expansion data and acoustic emission allow completing the analysis providing microstructure information versus temperature. Finally hypothesis concerning damage mechanisms are confirmed with microstructure investigations (SEM, EBSD) of samples observed at room temperature.

4.1. Elastic properties

4.1.1. Results

Elastic properties obtained during a heating and cooling treatment up to/from 1500 °C (after a first heating at this temperature) have been measured with two techniques (Fig. 5). The first one is the pulse echography technique, with a Young's modulus (E) obtained for a typical strain of 3.10^{-6}% and the second one is the tensile test. The Young's modulus is obtained by measuring the linear slope between 0 and +0.5 MPa during a tensile-compression test between +2 MPa and −2 MPa.

Young's modulus evolution obtained with the pulse echography technique and the tensile are described for a heat treatment at 1500 °C. The pulse echography measurement of the studied material has already been described elsewhere.[25] Seven main steps can be identified:

Domain 1: starting from room temperature, E obtained by pulse echography and the tensile test remains relatively constant up to the glassy transition temperature ($T_g \approx 890$ °C). The Young's modulus measured by tensile test begins to drop.
Domain 2: $E_{\text{echography}}$ is stable up to 1150 °C, i.e. the temperature of monoclinic to tetragonal transition of zirconia for heating. At this temperature, the Young's modulus falls down due to both intrinsic differences of elastic properties between monoclinic and tetragonal zirconia and probably also due to microdamage.

In the same temperature range, the Young's modulus measured by the tensile test falls down.
Domain 3: $E_{\text{echography}}$ increases up to 1250 °C, whereas $E_{\text{tensile test}}$ decreases progressively. It must be noticed that the value obtained at high temperature (up to 1300 °C) by ultrasonic measurements is influenced by phenomena of signal attenuation (low viscosity of the glassy phase).
Domain 4: from 1500 °C, and down to the reverse T → M transformation at about 1000 °C, the Young's modulus obtained by the two techniques increases in line with the viscosity of the glassy phase (stiffening). There is a narrow peak in $E_{\text{echography}}$

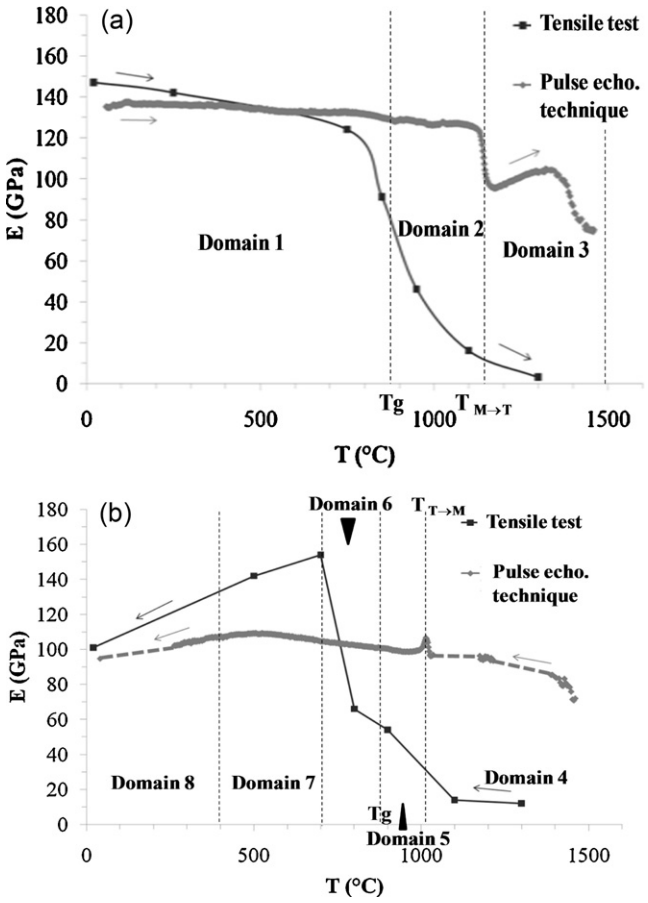

Fig. 5. Young's modulus evolution obtained by pulse echography method and tensile test during a heating treatment up to 1500 °C (a) and a cooling one from 1500 °C (b).

at the transformation temperature due in particular to the transformation T → M.

Domain 5: the Young's modulus slowly increases from 1000 °C to 890 °C. The progression is quicker for the tensile test measurement than for the pulse echography one.

Domain 6: E follows to increase down to 700 °C.

Domain 7: the linearity loss of $E_{echography}$ begins. It seems that the slope of $E_{echography}$ evolution decreases more slowly than the one of $E_{tensile\ test}$. This domain is defined in correlation with results obtained by acoustic emission and thermal expansion analysis presented below.

Domain 8: from 400 °C to room temperature, a significant decrease of E is observed.

4.1.2. Tensile test versus pulse echography technique: visco-plasticity evidence

It can be seen that elastic properties obtained by pulse echography and tensile test measurements are rather similar up to 750 °C. Above this temperature, Young's moduli obtained by tensile test decreases continuously when temperature increases. This effect is probably due to the fact that the glassy phase presents low viscosity properties above 890 °C (i.e. the vitreous transition temperature or T_g). As the T_g is in reality a range of temperature the effect can begin at a lower temperature.

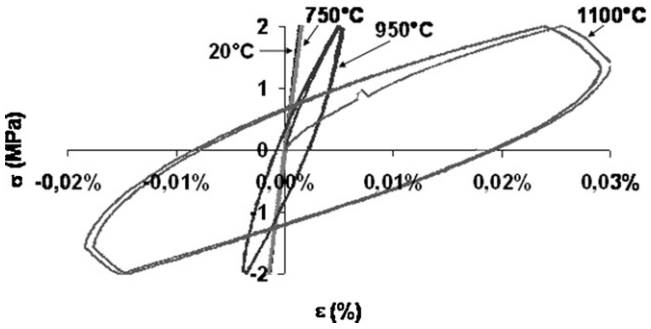

Fig. 6. Stress-strain behavior during tensile-compressive tests between 2 and −2 MPa at 20 °C, 750 °C 950 °C and 1100 °C during heating process.

In fact, as the material, in this range of temperature, does not exhibit an elastic behavior, the more important strain enhanced by the tensile test is responsible for a high dependence of the Young's modulus to the viscosity of the glassy phase. A look on successive tensile-compressive tests curves (Fig. 6) obtained by cycling between 2 and −2 MPa for different temperatures around 800 °C (20 °C, 750 °C, 950 °C and 1100 °C), confirms the low viscous behavior mainly due the glassy phase above 800 °C, i.e. the T_g.

The same effect can be observed in a reverse way during cooling from high temperature to 700 °C.

Considering now differences in Young's modulus values obtained down from 800 °C, two considerations must be taken into account:

- due to possible heterogeneities between samples (from a large block) and the fact that tensile test is only performed during cooling on one single sample, it is possible to have some fluctuation in absolute values between E measured with the two techniques.
- as the same sample is successively cycled between +2 MPa and −2 MPa for each testing temperature, the continuous decrease of E down from 800 °C is maybe due to both damage inherited from the thermal treatment and from the cumulative cycling test.

In the following part of the study, main realistic elastic properties will be considered to be issued from the ultrasonic method. Then, as the study aims to study the cooling process, authors will focus in the following part on the cooling treatment for acoustic emission and thermal expansion analysis.

4.2. Thermal expansion analysis and acoustic emission: investigations of microstructure evolution in temperature

Thermal expansion analysis and acoustic emission tests have been performed for the studied material (Fig. 7) during a cooling from 1500 °C. Firstly, two particular phenomena must be noticed concerning the thermal expansion curve:

- a large expansion on cooling at around 1000 °C due to the martensitic transformation of ZrO_2. This temperature is very closed to the one observed for the tetragonal to monoclinic

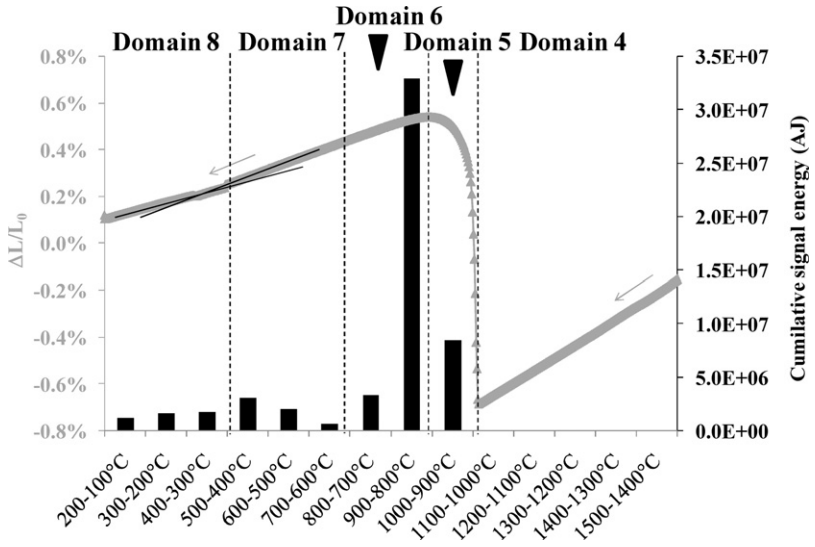

Fig. 7. Thermal expansion analysis and cumulative AE energy for each 100 °C temperature range during a cooling treatment down from 1500 °C.

transition of zirconia. The linear expansion measured here is of about 1.3% which is approximately in accordance with the 4 vol% of the literature.
- a change in the slope of the thermal expansion curve at around 450 °C. The coefficient of thermal expansion seems to decrease below this temperature.

To present AE data, the cooling process is divided into ranges of 100 °C. Evolution of the cumulative signal energy for each 100 °C range is plotted. Three main steps can be highlighted, referring directly to Young's modulus evolution:

Domain 4: few AE signal is recorded in this area. It must be considered that the low viscosity of the glassy phase is responsible for a strong attenuation of acoustic signals.
Domains 5 and 6: cumulative AE energy increases significantly in the range 900–800 °C but falls down drastically in the next 100 °C range.
Domain 7: values of cumulative energy increase progressively in the zone 700–400 °C. Nonetheless, maximum values obtained are much lower than those observed in the previous domain.
Domain 8: from 400 °C to 100 °C, a relative dwell is observed in AE energy.

As these two experiments express microstructure mechanisms, it is clear that microdamage evolves, following different steps, during the cooling stage. Using microstructure observations, the following part aims to discuss on possible involved microdamage mechanisms.

4.3. Identification of damage features at room temperature after the cooling process

Evidences of microcracking occurrence during the cooling stage can be observed in the studied fused-cast material. The location of these microcracks is various. Some of them are concentrated in the interface region between the glassy phase and zirconia dendrite branches (Fig. 7), and others are localized within zirconia dendrite branches themselves (Fig. 8).

These microcracks probably result from different process:

- The first ones located, as previously quoted, in the interface region between the glassy phase and zirconia dendrite branches (inter-branch microcracks) are most probably due to thermal expansion mismatches between zirconia and glassy phases. The observation of such microdamages (Fig. 8) is quite difficult to achieve because of they are not numerous. Anyway, a complementary thermal treatment at 1500 °C, increases their density and allows to see them more easily.
- The second ones so-called "intra-branch microcracks" are more related to expansion mismatches within zirconia dendrite branches themselves due to anisotropy of thermal expansion along crystallographic axis of each single domain. A special chemo-mechanical procedure of polishing (colloidal silica) coupled with SEM observations in Back Scattered Electrons mode (BSE) with a low H_2O pressure environment allows to reveal crystallographic contrasts in zirconia dendrite

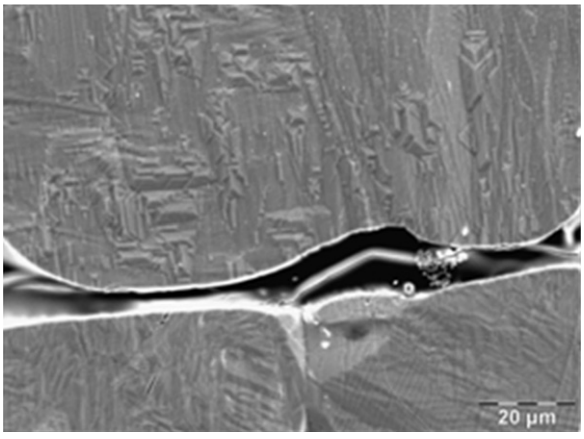

Fig. 8. SEM observation of inter-branch microcracks located in the glassy phase.

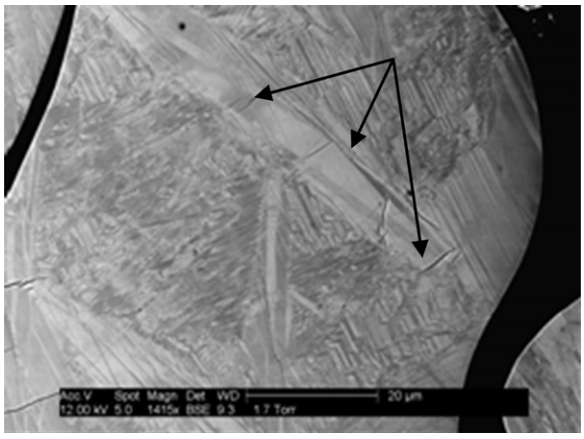

Fig. 9. SEM observation in BSE mode (low H_2O vapor environment) of intra-branch microcracks in a zirconia dendrite branch.

branches. Domains can be observed in each branch with microcracks located along or inside these domains (Fig. 9).

These domains, revealed by the BSE mode, are related to crystallographic monoclinic variants. Classical microstructure observations like SEM or optical observations do not permit easily to identify crystallographic features at a low scale. This is the reason why authors use EBSD experiments in the present study to map zirconia dendrites and understand the link between crystallographic variants and the occurrence of microcracking. An EBSD map with four main types of crystallographic orientations (i.e. four different variants with one point for each variant) is presented in Fig. 10. The corresponding direct pole figure of the $\{1\,0\,0\}$, $\{0\,1\,0\}$ and $\{0\,0\,1\}$ planes are drawn in the same figure with the same contrasts corresponding to the same orientations. Authors will not go in the details of variants identifications and suggest to refer to others paper for further information concerning the classification of monoclinic variants of zirconia.[6] Here, we only suggest to focus on the link between the crystallographic axes of the monoclinic variants (with the corresponding thermal expansion) and the way of microcracking occurrence. If we focus on the monoclinic pole figure $\{0\,0\,1\}$, i.e. the projection of normals to the family planes $\{0\,0\,1\}$ (i.e. approximately the monoclinic c axis), it can be seen for each of the four types of variants, that c axis seem to be perpendicular to the microcracking planes for a given domain (or group of variants with the same orientation). Indeed, It is well-known that the c_m axis exhibits the largest thermal expansion coefficient ($\sim 12\,K^{-1}$), compared to a_m and b_m axis ($8\,K^{-1}$ and $3\,K^{-1}$ respectively).[25] Then, it explains how anisotropic thermal expansion between crystallographic axes can induce microcracking phenomena within a given variant. In the same way, microcracks are also generated along large domains (i.e. between different variants), due to thermal expansion mismatches between crystallographic variants.

Two types of microcracking occurrence (inter-branch and intra-branch microcracks) are thus relative to different microdamage mechanisms. The difficulty here is to identify the chronology of damage occurrence during the cooling process. One can easily imagine that the occurrence of the zirconia martensitic transformation and the evolution of the viscosity of the glassy phase play a major role in the chronology of mechanisms.

4.4. Discussion

These results highlight three types of microstructural effects which play major roles in the thermomechanical behavior during thermal cycles at high temperature: the viscosity of the glassy phase, the $M \leftrightarrow T$ transformation of zirconia and the microdamage evolution. These effects are interdependent and are suspected to be particularly important during the cooling step of processing (annealing).

Authors suggest to split the discussion into four temperature range: a very high temperature domain (1500–1000 °C) or Domain 4, a high temperature domain (1000–800 °C) or Domains 5 and 6, a medium temperature area (800–400 °C) or Domain 7 and a low temperature one (400–100 °C) or Domain 8.

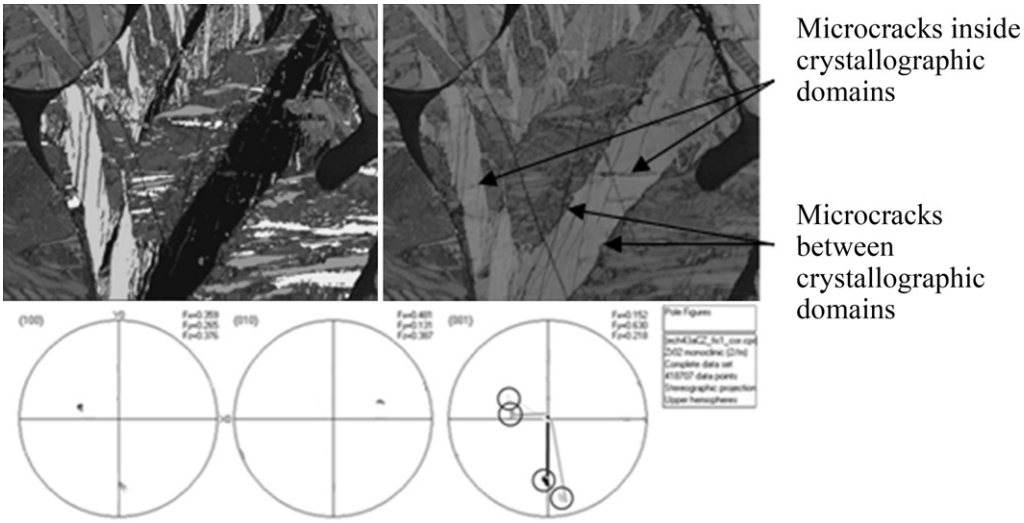

Fig. 10. EBSD map of inter-branch microcracks in the glassy phase.

4.4.1. Very high temperature domain: 1500–1000 °C (Domain 4)

The low viscosity of the glassy phase, responsible for the attenuation of acoustic signals, does not allow to extract clear information about microdamage. It can only be assumed that no microcracks occur in this domain, considering that the glassy phase can accommodate stresses.

4.4.2. High temperature domain: 1000–700 °C (Domains 5 and 6)

Measurements of viscosity evolution on glass synthetic samples (same composition as the glassy phase of the studied material) have shown that the glass transition temperature T_g is at about 800 °C.[26] Thus, between 1000 °C and 800 °C, the glassy phase is in a low viscous state. It is then assumed that a strong attenuation of the signals exists, linked to the evolution of the glassy phase viscosity. This phenomenon explains partially the progressive increase of cumulative AE energy, i.e. the glassy phase behaves like a low-pass filter. Above T_g, microdamage mechanisms responsible for the narrow peak in Young's modulus evolution are mainly relative to rubbing phenomena between zirconia dendrite branches and the generation of zirconia variants with the associated intra-branch microcracks (T → M transformation in zirconia). In fact, the glassy phase is not enough viscous to allow the formation of microcracks. Observation of AE data shows that during the range 900–800 °C, the maximum of cumulative signal energy of the whole cooling process is observed. It means that it is possible that attenuation hides part of signals above 800 °C and so does not permit to identify rigorously some maximum in damage occurrence between 1000 °C and 800 °C.

A look at the number of cumulative hits on the different ranges of temperature in the Table 1 and evolution of cumulative signal energy is then of a great interest. In fact, it shows that energy and the number of hits strongly decrease in the range 800–700 °C.

Microdamage effects are probably dominant as soon as the glassy phase viscosity go through a low viscosity state at T_g (between 900 °C and 800 °C). There is then probably a mix of intra-branch microcracking phenomena, rubbing (wear) between dendrite branches and the glassy phase. In the range 800–700 °C, it could shift to less intra-branch microcracking phenomena and so the majority of signals could be created by rubbing phenomena. If the hypothesis is correct, it means that rubbing phenomena are less energetic than intra-branch microcracks. In fact, the number of cumulative hits is only the third in the range 800–700 °C compared to the previous range whereas the cumulative energy is approximately seven times lower. This is consistent with the empirical bursting character of microcracks versus rubbing.

4.4.3. Medium temperature domain: 700–400 °C (Domain 7)

The signal energy continues to drop from 800–700 °C to 700–600 °C. This is accompanied by a large decrease of the number of hits. Then, cumulative AE energy increases continuously between 600 °C and 400 °C. It can be seen at around 700 °C a loss of linearity in Young's modulus evolution which is

Table 1
Number of cumulative hits associated to each 100 °C temperature domains during the cooling stage.

Temperature range	1500–1400 °C	1400–1300 °C	1300–1200 °C	1200–1100 °C	1100–1000 °C	1000–900 °C	900–800 °C	800–700 °C	700–600 °C	600–500 °C
Cumulative hits	0	0	0	0	61	2327	7896	2981	1303	1123

considerably reinforced below 500 °C. At the same time, a slope change in the thermal expansion curve is observed at around 450 °C. This medium temperature range is probably the beginning of another step of microdamage or coalescence of existing microcracks. In fact, since the glassy phase is completely solidified, CTE mismatches between zirconia grains and the glassy phase and between zirconia grains themselves are probably responsible for a progressive increasing of the stress field especially around zirconia particles. As the number of hits is quite stable in this range, initiation mechanisms which are quick phenomena are maybe replaced by mechanisms of microcrack propagation and enlargement with lower energy parameters.

4.4.4. Low temperature range: 400–100 °C (Domain 8)

The Young's modulus drops continuously down to 100 °C and no sensitive variation of cumulative signal energy is recorded. Mechanisms of microcrack propagation follow in a regular way in the material. The material becomes more and more damaged at very small scale.

5. Conclusion

This paper aims to study microdamage occurrence during a cooling process down from 1500 °C, using a set of different techniques working at high temperature. A parallel, between elastic properties obtained by two different ways and both thermal expansion analysis and acoustic emission performed at high temperature, allows to link the mechanical behavior to microstructure changes. The fused cast material studied presents a rather complex microstructure due to the way of casting and successive transformations of zirconia. It is the reason why an original device called EBSD is used here to characterize crystallographic orientations in relation with damage occurrence coupled with SEM investigations. In particular, a direct link between intra-branch microcracking and organization of zirconia variants has been highlighted. The correlation between all the techniques allows establishing hypothesis about the chronology and nature of microdamage mechanisms. From an applicant point of view, such microcracks does not affect performances of materials at operating temperature for glass manufacturing because they are for the most part recovered.

Four domains of temperature have been emphasized during the cooling stage to explain the process of occurrence of intra-branch and inter-branch microcracking, by taking into account the low viscosity state of the glassy phase at high temperature (revealed by tensile-compressive tests), the martensitic transformation of zirconia at around 1000 °C and the glassy phase transition at about 800 °C. No real information can be extracted from the first very high temperature domain (1500–1000 °C) due to the attenuation of acoustic signals created by the low viscous behavior of the glassy phase. The second domain (1000–700 °C) corresponds mainly to intra-branch microcracking and some rubbing phenomena due to the transformation $T \rightarrow M$ of zirconia and the formation of crystallographic variants just after the temperature of transition and the solidifying process of the glassy phase which becomes rather elastic at around 800 °C. The medium temperature range (700–400 °C), especially around 500 °C, is probably the onset of another type of microdamage or the propagation of an existing one. In fact, since the glassy phase is completely solid, CTE mismatches between zirconia dendrite branches and the glassy phase and between variants within zirconia dendrite branches themselves are probably responsible for a progressive increasing of the stress field especially around zirconia dendrites. Finally, in the low temperature domain from 400 °C to room temperature, mechanisms of microcrack propagation follow in a regular way in the material. The material becomes more and more microdamaged. The "experimental characterization package" (ultrasonic pulse echography, tensile test, thermal expansion technique, acoustic emission monitoring) presented here appears to be a powerful set of techniques to correlate microstructure phenomena occurring during heat treatments to macroscopic effects, for example mechanical properties. Some other technique acting at crystal scale (EBSD) can efficiently support this package leading to a global interpretation of phenomena within the material.

In a near future, a deeper investigation will be devoted to flaw identification in order to correlate the type of recorded signal with observed damage within the material. From this point, an acoustic signature characterization demarche will be carried out.

Acknowledgements

Authors are greatly thankful to Saint-Gobain High Performance Materials, industrial partner in NOREV program, for supplying the materials, to the French National Research Agency (ANR) for its financial support and to Thierry Douillart for his help for ESEM observations.

References

1. Duvierre G, Boussant-Roux Y, Nelson M. Fused zirconia or fused AZS: which is the best choice? *Ceram Eng Sci Proc* 1999;**20**(1): 65–72.
2. Zanoli A, Duvierre G, Sertain G. High zirconia fused-cast refractories: a solution to defect and corrosion problems in special glasses. *Ceram Eng Sci Proc* 1991;**12**(3–4):496–517.
3. Madi K. Influence de la morphologie tridimensionnelle des phases sur le comportement mécanique de réfractaires électrofondus. PhD thesis. France: ENSMP; 2006.
4. Butterman WC, Foster DR. Phase diagram for ceramists. *Am Ceram Soc* 1974 [Colombus, fig. 2400].
5. Kelly KM, Francis Rose LR. The martensitic transformation in ceramics – its role in transformation toughening. *Prog Mater Sci* 2002;**47**: 463–557.
6. Sakuma K. Microstructural aspects on the cubic–tetragonal transformation in zirconia in Zirconia engineering ceramics – old challenges, new ideas. *Key engineering materials*, vol. 153–154. Switzerland: Trans. Tech. Publications; 1998. p. 75–96.
7. Buljan ST, McKinstry HA, Stubican VS. Optical and X-ray single crystal studies of the monoclinic–tetragonal transition in ZrO_2. *J Am Ceram Soc* 1976;**59**(7–8):351–4.
8. Huger M, Fargeot D, Gault C. High-temperature measurement of ultrasonic wave velocity in refractory material. *High Temp – High Pres* 2002;**34**:193–201.
9. Kakroudi MG, Huger M, Gault C, Chotard T. Anisotropic behaviour of andalusite particles used as aggregates on refractory castables. *J Eur Ceram Soc* 2009;**29**(4):571–9.

10. Standard terminology for non-destructive examination. E1316-96, Non-destructive testing. In: Annual book of ASTM standards, vol. 03.03; 1996, p. 609.
11. Hamstad MA, Thompson PM, Young RD. Flaw growth in alumina studied by acoustic emission. *J Acoust Emis* 1987;**6**:93–7.
12. Bakuckas JG, Prosser WH, Johnson WS. Monitoring damage growth in titanium matrix composites using acoustic emission. *J Comp Mater* 1994;**28**:305–28.
13. Berkovits A, Fang D. Study of fatigue crack characteristics by acoustic emission. *Eng Fract Mech* 1995;**51**:401–16.
14. Havlicek F, Crha J. Acoustic emission monitoring during solidification processes. *J Acoust Emis* 1999;**17**:3–4.
15. Coddet C, Chretien JF, Beranger G. Investigation on the fracture mechanism of oxide layers growing on titanium by acoustic emission. *Titanium and Titanium Alloys: Sci Technol Aspects* 1982;**2**:1097–105.
16. Barré S, Benzeggagh ML. On the use of acoustic emission to investigate damage mechanisms in glass-fibre-reinforced polypropylene. *Comp Sci Technol* 1994;**52**:369–76.
17. Suzuki H, Takemoto M, Ono K. The fracture dynamics in a dissipative glass fibber/epoxy model composite with AE source simulation analysis. *J Acoust Emis* 1996;**14**:35–50.
18. Pauchard V, Brochado S, Chateauminois A, Campion H, Grosjean F. Measurement of sub-critical crack-growth rates in glass fibbers by means of acoustic emission. *J Mater Sci Lett* 2000;**19**:2141–3.
19. Chotard T, Smith A, Rotureau D, Fargeot D, Gault C. Acoustic emission characterisation of calcium aluminate cement hydration at an early stage. *J Eur Ceram Soc* 2003;**23**:387–98.
20. Chotard T, Quet A, Ersen A, Smith A. Application of the acoustic emission technique to characterise liquid transfer in a porous ceramic during drying. *J Eur Ceram Soc* 2006;**26**:1075–84.
21. Chotard T, Soro J, Lemercier H, Huger M, Gault C. High temperature characterization of Cordierite–Mullite refractory by ultrasonic means. *J Eur Ceram Soc* 2008;**28**:2129–35.
22. Briche G, Tessier-Doyen N, Huger M, Chotard T. Investigation of damage behaviour of refractory model materials at high temperature by combined pulse echography and acoustic emission techniques. *J Eur Ceram Soc* 2008;**28**:2835–43.
23. Humphreys FJ. Grain and subgrain characterisation by electron backscatter diffraction. *J Mater Sci* 2001;**36**:3833–54.
24. Gey N, Humbert M. Specific analysis of EBSD data to study the texture inheritance due to the$\beta \rightarrow \alpha$ phase transformation. *J Mater Sci* 2003;**38**:1289–94.
25. Patapy C, Gault C, Huger M, Chotard T. Acoustic characterization and microstructure of high zirconia electrofused refractories. *J Eur Ceram Soc* 2009;**29**(16):3355–4336.
26. Yeugo Fogaing Y. High temperature characterisation of the elastic properties of fused-cast refractories and refractory castables. PhD thesis. University of Limoges; 2007.